

Nonequilibrium Rashba field driven domain wall motion in ferromagnetic nanowires

Martin Stier,¹ Reinhold Egger,² and Michael Thorwart¹

¹*I. Institut für Theoretische Physik, Universität Hamburg, Jungiusstraße 9, 20355 Hamburg, Germany*

²*Institut für Theoretische Physik, Heinrich-Heine-Universität Düsseldorf, 40225 Düsseldorf, Germany*

We study the effects of spin-orbit interaction (SOI) on the current-induced motion of a magnetic (Bloch) domain wall in ultrathin ferromagnetic nanowires. The conspiracy of spin relaxation and SOI is shown to generate a strong nonequilibrium Rashba field, which can dominate even for weak SOI. This field causes intricate spin precession and a transition from translatory to oscillatory wall dynamics with increasing SOI. We show that current pulses of different lengths can be used to efficiently control the domain wall motion.

PACS numbers: 75.78.Fg, 75.70.Tj, 75.25.-b

I. INTRODUCTION

The efficient and reliable manipulation of magnetic microstructures forms the basis for most information storage devices used nowadays. Commonly, an applied local magnetic field controls the magnetization in a given domain. The alignment direction encodes a classical bit, and the data storage density is limited by the domain size. Recent advances in nanofabrication have implemented Berger's proposal¹ of moving a domain wall (DW) by a current-induced spin torque². This may allow for ultrasmall magnetic devices with high data storage density in ferromagnets carrying a spin-polarized current. The local magnetization can be electrically controlled by a spin torque arising from the exchange coupling of the local spins to conduction electron spins. Across a wide DW, the polarization of the itinerant spins adiabatically follows the magnetization direction, angular momentum is transferred due to total spin conservation, and DW motion along the current direction is induced. In addition to this adiabatic spin torque², a nonadiabatic spin torque plays a prominent role³⁻⁷: This so-called “ β -term” is due to spin relaxation, which causes the itinerant spin polarization to “lag” behind the local magnetization. This nonequilibrium contribution to the torque critically determines the DW velocity and shape, as well as the depinning and critical (Walker breakdown) current densities.

Ferromagnetic nanowires are natural candidates for building ultrafast memory and logic devices that rely on nanoscale current-induced DW motion. While quite high DW velocities (≈ 100 m/s) are possible in permalloy (NiFe) nanowires^{8,9}, these setups often suffer from limited reproducibility, strong DW pinning, and low critical currents. Following earlier proposals^{10,11}, recent experiments¹² realized Co nanowires in an $\text{AlO}_x/\text{Co}/\text{Pt}$ trilayer structure, where structural inversion asymmetry causes an interfacial electric field and thus a Rashba spin-orbit interaction (SOI)¹³. This electronic SOI is strong, can be tuned by electrostatic gating, and allows one to largely circumvent the above problems^{12,14,15}. The observed DW velocities of up to 400 m/s (and other interesting features, e.g., DW motion against the current direction) were attributed¹² to a conspiracy of the β -term and

a field-like adiabatic Rashba spin torque^{10,11,16-20}, denoted \mathbf{T}_1 below. While \mathbf{T}_1 does not involve spin transfer and can be traced back to the electronic bandstructure, it depends on the current and can switch the magnetization. These exciting experimental observations and their technological promise have triggered further theoretical works²¹⁻²⁵, which draw a more complex picture, involving also a Slonczewski-type nonadiabatic Rashba spin torque (denoted \mathbf{T}_2 below) due to the interplay of SOI and spin relaxation occurring under nonequilibrium conditions.

Given the complexity of this problem, we here aim to understand current-induced DW motion in a ferromagnetic Rashba nanowire in the simpler one-dimensional (1D) limit. This limit allows for the analytical calculation of the full current-induced nonadiabatic spin torque appearing in the Landau-Lifshitz-Gilbert (LLG) equation for the space- and time-dependent magnetization profile. Previous experiments¹² have used Co nanowires of diameter ≈ 500 nm, much thicker than the few-channel nanowires studied here, but future experiments could approach this ultrathin-wire limit. By numerical solution of the LLG equation including the full spin torque, with the nanowire initially containing a Bloch DW, we predict ultrafast DW velocities in current-pulsed setups. Surprisingly, we find that already weak Rashba spin-orbit couplings have a huge effect on the DW dynamics due the appearance of a “nonequilibrium Rashba field.” Spin-orbit coupled ferromagnetic nanowires are thus predicted to allow for ultrafast and efficient DW dynamics.

II. MODEL AND LLG EQUATION

We here study an ultrathin ferromagnetic Rashba nanowire (along the x -direction), where localized spins create the magnetization profile $-M_s \mathbf{n}(x, t)$, with unit vector \mathbf{n} and saturation magnetization M_s . The magnetization dynamics is governed by the LLG equation²,

$$\partial_t \mathbf{n} = -\mathbf{n} \times \mathbf{H}_{\text{eff}} + \alpha \mathbf{n} \times \partial_t \mathbf{n} + \mathbf{T}, \quad (1)$$

where the effective field $\mathbf{H}_{\text{eff}}(x)$ generates magnetic texture (for a specific DW profile, see below) in the absence

of a current, and the Gilbert damping parameter α depends on intrinsic material properties. The spin torque, $\mathbf{T}(x, t)$, encapsulates all current-induced contributions due to the exchange interaction between localized moments and itinerant electrons, described here within the standard *sd* model. The conduction electrons carry a spin-polarized electric current, and also experience the Rashba SOI. Remarkably, in the 1D limit, analytical results for the full spin torque can be obtained by employing the textbook Sugawara representation²⁶. We discuss the main steps of the derivation next (we often use units with $\hbar = 1$). Technical details can be found in the Appendix .

III. DERIVATION

At low energy scales, itinerant electrons in the nanowire have linear momentum $k_x \approx pk_F$, where $p = +$ ($p = -$) stands for a right (left) mover and k_F is the Fermi momentum. Away from the band bottom, the dispersion relation can be linearized, where the Fermi velocity v sets the slope. The electronic spin density vector, $\mathbf{s}(x) = \mathbf{J}_R + \mathbf{J}_L$, and the corresponding spin current, $\mathbf{J}(x) = v(\mathbf{J}_R - \mathbf{J}_L)$, are thereby expressed in terms of chiral spin density vectors $\mathbf{J}_{R,L}(x)$ for p -movers only. Similarly, the (scalar) density, $\rho_c = \rho_R + \rho_L$, and the charge current flowing through the nanowire, $I_c = ev(\rho_R - \rho_L)$, follow from the chiral particle densities $\rho_{R,L}$. This separation into left- and right-moving parts is typical for 1D systems and allows for the analytical progress reported here. With the exchange coupling Δ_{sd} , the spin torque in Eq. (1) is $\mathbf{T}(x, t) = -\Delta_{sd}\mathbf{n} \times \langle \mathbf{s} \rangle$, where the average is over the electronic degrees of freedom taking into account the SOI. Using the dimensionless Rashba coupling α_R , the single-particle Hamiltonian receives the contribution $(\Delta_{sd}\alpha_R/2k_F)[\sigma_y k_x - \sigma_x k_y]$ ²⁷, where $\sigma_{x,y}$ are spin Pauli matrices and the channel-mixing term $\propto k_y$ is negligible for ultrathin nanowires²⁸. As discussed below, \mathbf{T} follows by solving the Heisenberg equations of motion for \mathbf{J}_p (with $p = +, - = R, L$),

$$(\partial_t + pv\partial_x)\mathbf{J}_p = -\Delta_{sd}\mathbf{J}_p \times (\mathbf{n} + p\alpha_R\mathbf{e}_y) - \sum_{\nu=i,ii} \beta^{(\nu)}\Delta_{sd}(\mathbf{J}_p - \mathbf{J}_p^{(\nu)}), \quad (2)$$

where spin relaxation (the last term) has been included phenomenologically within the relaxation-time approximation; \mathbf{e}_y is the unit vector in the y -direction. We identify two competing relaxation mechanisms characterized by different stationary configurations, $\mathbf{J}_p^{(i)}$ and $\mathbf{J}_p^{(ii)}$, and different rates governing the relaxation into them, $\beta^{(i)}\Delta_{sd}$ and $\beta^{(ii)}\Delta_{sd}$, respectively. Mechanism (i) arises due to the contact of the nanowire to ferromagnetic leads, which inject the spin-polarized current $I_s = \hbar PI_c/2e$ with spin polarization factor $-1 \leq P \leq 1$ ²⁹. Fluctuations then try to establish the stationary distribution $\mathbf{J}_p^{(i)} = \frac{1}{2}P\rho_p\mathbf{n}$ ³⁰. Mechanism (ii) instead describes spin

relaxation to the intrinsic stationary solution of Eq. (2), $\mathbf{J}_p^{(ii)}(x) = \frac{1}{2}P\rho_p[\mathbf{n}(x) + p\alpha_R\mathbf{e}_y]$.

For a given magnetization profile $\mathbf{n}(x, t)$, since the typical space-time variations of \mathbf{n} are slow compared to electronic variations, Eq. (2) can now be solved analytically by an iterative gradient expansion⁵. In this approach, we first determine the spin torque under the assumption that all space-time derivatives $\partial_{x,t}\mathbf{n}$ can be discarded. The resulting zeroth-order result, $\mathbf{T} = \mathbf{T}^{(0)}(x, t)$, is then used to obtain the first-order correction to the spin torque, $\mathbf{T}^{(1)}$, calculated by retaining terms $\sim \partial_{x,t}\mathbf{n}$ but omitting all higher derivatives. We consider only those two orders and, for clarity, we write down only the leading terms in $\alpha_R \ll 1$ below. Complete spin torque expressions, valid for arbitrary α_R , are lengthy and given in the Appendix . Our numerical results for the DW dynamics (see below) were obtained with the complete expressions but remain very similar when using only the small- α_R spin torque.

IV. CURRENT-INDUCED RASHBA SPIN TORQUE

We recover the two Rashba spin torques discussed in the Introduction already from the zeroth-order result, $\mathbf{T}^{(0)} = \mathbf{T}_1 + \mathbf{T}_2$. The field-like spin torque, $\mathbf{T}_1 = -\mathbf{n} \times \mathbf{H}_R$, can be written in terms of a “nonequilibrium Rashba field,”

$$\mathbf{H}_R = H_R^{(0)}\mathbf{e}_y, \quad H_R^{(0)} = \alpha_R I_s \Delta_{sd}/v, \quad (3)$$

while the Slonczewski-type nonadiabatic Rashba spin torque reads

$$\mathbf{T}_2 = (\beta^{(i)}\alpha_R I_s \Delta_{sd}/v)\mathbf{n} \times (\mathbf{n} \times \mathbf{e}_y). \quad (4)$$

The structure of both spin torques agrees with previous results^{21–25}. For the first-order correction $\mathbf{T}^{(1)}$, we have

$$\mathbf{T}^{(1)} = -I_s\partial_x\mathbf{n} + \beta^{(i)}I_s\mathbf{n} \times \partial_x\mathbf{n} - H_R^{(1)}\mathbf{n} \times \mathbf{e}_y, \quad (5)$$

where additional time-dependent terms $\sim \partial_t\mathbf{n}$ (not shown) effectively renormalize the Gilbert damping parameter. In Eq. (5), we recognize the adiabatic spin torque (first term) as well as the “ β -term” (second term), where both are present already without SOI. Finite α_R then renormalizes the prefactors in both terms (see Appendix). The last term in Eq. (5) contributes to the nonequilibrium Rashba field, $\mathbf{H}_R = H_R\mathbf{e}_y$ with $H_R = H_R^{(0)} + H_R^{(1)}$, where we find

$$H_R = \frac{\alpha_R I_s \Delta_{sd}}{v} - \frac{\alpha_R^2 \beta^{(ii)} I_s}{(\beta^{(i)} + \beta^{(ii)})^2} \partial_x n_y + \mathcal{O}(\alpha_R^3). \quad (6)$$

The first term comes from Eq. (3) and has been discussed before^{10,11,16–20}. The second term in Eq. (6) is new and may dominate for $\beta^{(i,ii)} \ll \alpha_R^2$. This implies that a strong nonequilibrium Rashba field already emerges even for rather weak Rashba couplings. While nonadiabatic

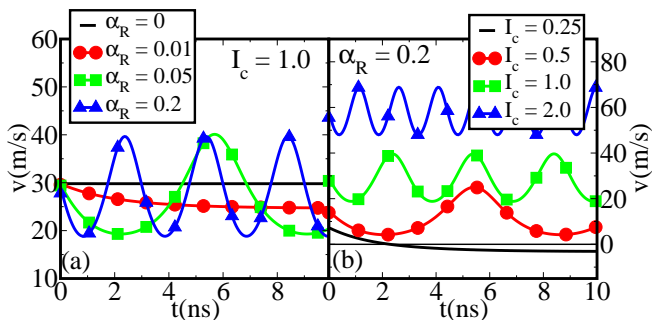


FIG. 1. (Color online) Velocity of the DW center vs propagation time for (a) different α_R and (b) different I_c (10^{12} A/m 2). An increase of either α_R or I_c increases the Rashba field H_R . At the critical value H^{WB} , we find a current-induced Walker breakdown and the velocity starts to oscillate. Further increase of α_R or I_c increases the oscillation frequency.

torque contributions [T_2 in Eq. (4) and the second term in Eq. (5)] are due to relaxation mechanism (i), $H_R^{(1)}$ is mainly caused by mechanism (ii)³¹.

V. NUMERICAL SIMULATION

To obtain explicit results for the current-induced DW motion, we have performed numerical simulations. We study a Bloch- y DW created by the effective magnetic field $\mathbf{H}_{\text{eff}} = J\partial_x^2 \mathbf{n} + Kn_y \mathbf{e}_y - K_\perp n_x \mathbf{e}_x$ in Eq. (1), where J is an exchange coupling between localized moments, K and K_\perp are anisotropy constants. Measuring length (time) in units of $x_0 = 0.5$ nm ($t_0 = 1$ ps), we adopt the following parameter values: $J = 5.2$, $K = 0.185$, $K_\perp = 0.008$, $\alpha = \beta^{(i)} = \beta^{(ii)} = 0.06$. This choice corresponds to Ta/CoFeB/MgO, a material with comparably strong SOI as in Co nanowires and well characterized parameter values¹⁷. Furthermore, unless stated otherwise, we set $\Delta_{\text{sd}}/v = 0.2$, $v = 2 \times 10^5$ m/s, $\alpha_R = 0.2$, $P = 1$, $\rho_c = I_c/v$, and $I_s = 0.06$. The latter value implies a charge current density $I_c = 10^{12}$ A/m 2 . We have verified from additional calculations for other parameter sets (not shown) that the results below are generic.

A. Steady-state current

Numerical solution of Eq. (1) with a time-independent current density I_c confirms that the DW motion is strongly influenced by the Rashba SOI, both concerning the instantaneous (momentary) motion and the asymptotic long-time behavior. Let us first discuss the time evolution of the momentary velocity, see Fig. 1. With increasing SOI strength α_R , we observe a transition from purely translatory motion, with (asymptotically) constant DW velocity, to a regime with superimposed oscillations in the time-dependent velocity. Our numerical analysis reveals that the oscillations stem mainly from

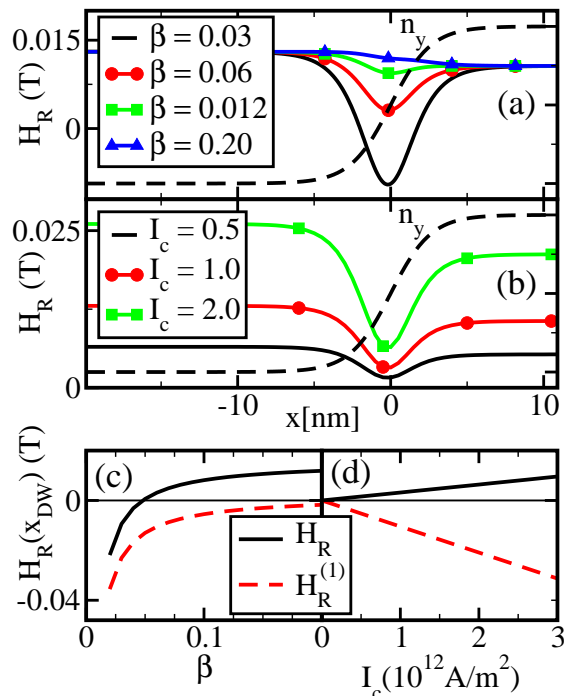


FIG. 2. (Color online) Momentary Rashba field H_R (in Tesla) close to the DW center (taken at $x_{DW} = 0$). We put $\alpha = \beta^{(i)} = \beta^{(ii)} \equiv \beta$ and show the behavior for (a) different β (with $I_c = 10^{12}$ A/m 2), and (b) for different current densities I_c (in 10^{12} A/m 2), with $\beta = 0.06$. For comparison, the n_y -component of the magnetization is shown as dashed curve. The last two panels illustrate the Rashba field $H_R(x_{DW})$ and the contribution $H_R^{(1)}$ directly at the DW center: (c) H_R vs β , and (d) H_R vs I_c .

the Rashba field \mathbf{H}_R . In fact, the DW magnetization \mathbf{n} is found to precess around the y -axis, which is the direction of the Rashba field (cf. Appendix). This behavior strongly resembles a *field-induced* Walker breakdown, where the oscillations appear once H_R exceeds a certain critical Walker field H^{WB} . As is known from the field-induced case, this critical field depends on the perpendicular anisotropy, $H^{WB} \propto K_\perp$ ³². Within the regime $H_R > H^{WB}$, we observe that the oscillation amplitude increases with K_\perp , but remains independent of all other parameters, while the oscillation frequency is $\propto H_R$. Since H_R is affected by a spin-polarized current I_s and not only by α_R , the DW motion can be effectively controlled by I_s , see Fig. 1(b). The impact of all other parameters on the DW motion is less pronounced and not discussed here.

B. Nonequilibrium Rashba field

The spatial distribution of the momentary Rashba field, $H_R(x)$, is illustrated in Fig. 2. We focus on the most relevant behavior of this field close to the DW center. Near the DW center, $\partial_x n_y$ is sizable, and we then

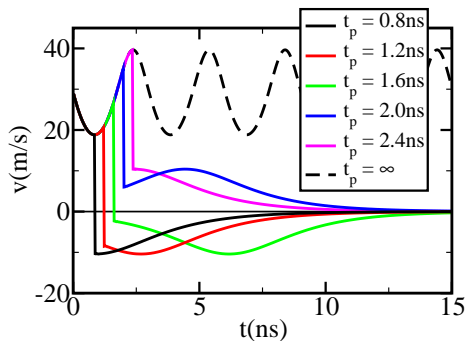


FIG. 3. (Color online) Velocity of the DW center vs propagation time for five current pulses of different length t_p . After the pulse, the DW drifts for a certain time in either positive or negative direction (depending on the oscillation phase at the pulse end). The dashed curve shows the corresponding result for a steady-state current.

find that $H_R^{(1)}$ dominates as long as the damping parameter β stays small, in accordance with Eq. (6). Far away from the DW center, as expected, $H_R^{(1)}$ plays no significant role. Similarly, for large β , Fig. 2(c) demonstrates that the contribution $H_R^{(1)}$ is suppressed against $H_R^{(0)}$, cf. Eq. (3). For sufficiently small but finite β , we find that $H_R^{(1)}$ always provides the dominant contribution to the nonequilibrium Rashba field near the DW center.

C. Domain wall response to current pulses

Experiments are often carried out with current pulses instead of steady-state currents^{12,33}. For rectangular current pulses of duration t_p , we find that current-induced DW motion closely resembles the behavior in the field-driven case above the Walker breakdown². Here, the DW does not immediately stop at the end of the pulse, but instead *drifts* for a certain time with nearly constant velocity, see Fig. 3. Interestingly, the drift direction depends on the actual phase of the oscillation at the end of the pulse. Therefore, even if the DW initially moves forward due to the current pulse, it may still end up in a backward position relative to its starting point. For short current pulses, the drifting mechanism can completely dominate the total DW displacement.

D. Global average wall velocity

In the current-pulsed case, a straightforward way to determine the average DW velocity is to measure the initial and final DW position before and directly after the pulse, and then to divide this distance by the pulse duration t_p ³². In experiments, however, it is often difficult to read out the DW position right at the end of the pulse, and usually one obtains the final position only somewhat later. The extracted average velocity thus coincides with

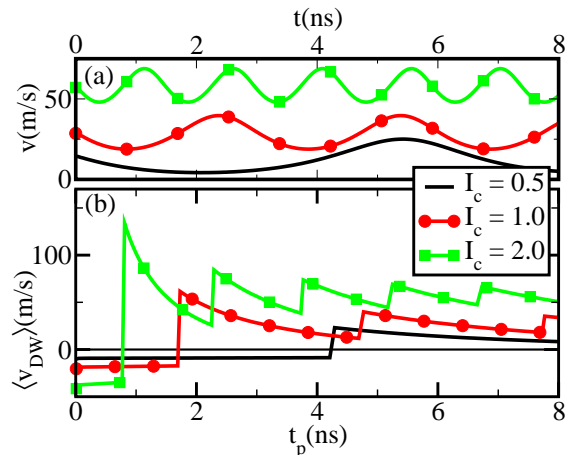


FIG. 4. (Color online) (a) Momentary velocity of the DW center vs propagation time for a steady-state current. (b) Average DW velocity $\langle v_{DW} \rangle = x_{DW}(t \rightarrow \infty)/t_p$ vs current pulse duration t_p with I_c (10^{12} A/m²). Depending on the momentary velocity at the pulse end, the DW drifts in different directions. Especially for short pulses, this may strongly affect $\langle v_{DW} \rangle$.

the real one only if the DW stops instantly when the pulse ends. Figure 3 demonstrates that such assumptions are not valid in general: The final position, $x_{DW}(t \rightarrow \infty)$, typically deviates strongly from the location right after the pulse, $x_{DW}(t_p)$. In the following, we study the experimentally more accessible “global” average DW velocity, $\langle v_{DW} \rangle = x_{DW}(t \rightarrow \infty)/t_p$. A major issue determining $\langle v_{DW} \rangle$ is the oscillation phase reached by the DW at time $t = t_p$. With changing t_p , the oscillatory DW magnetization ends up in different configurations associated with different drift directions and final positions, $x_{DW}(t \rightarrow \infty) = x_{DW}(t_p) + x_{\text{drift}}$. While $x_{DW}(t_p) \sim t_p$ is determined by the pulse duration, x_{drift} can have either sign. For very long pulses ($t_p \rightarrow \infty$), we have $|x_{DW}(t_p)| \gg |x_{\text{drift}}|$, and the conventional average velocity, $x(t_p)/t_p$, coincides with $\langle v_{DW} \rangle$. For short pulses, however, they may differ considerably. We find that the t_p -dependence of the global average velocity $\langle v_{DW} \rangle$ exhibits a sawtooth-like behavior, see Fig. 4.

Tuning the pulse duration t_p is not the only way to control the motion of the DW. For fixed t_p , we can also change the oscillation frequency of the DW motion by changing the current density I_c , see Fig. 5. We again find a sawtooth-like dependence of $\langle v_{DW} \rangle$ on I_c , which roughly oscillates around the velocity found for $\alpha_R = 0$. For small values of I_c , the DW even moves against the current flow. Due to the strong I_c -dependence of $\langle v_{DW} \rangle$, small changes in the current can here lead to completely different types of DW motion.

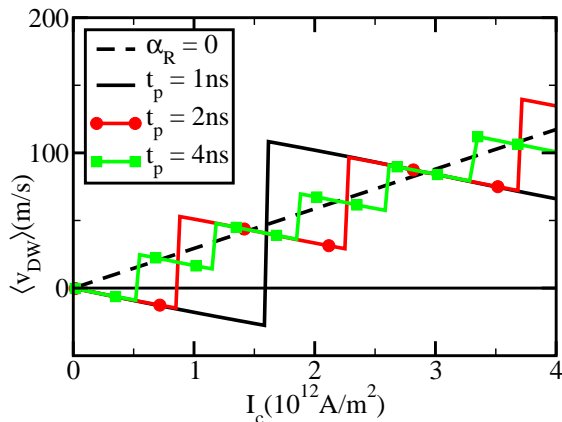


FIG. 5. (Color online) Global average velocity of the DW center $\langle v_{DW} \rangle$ vs current density I_c for fixed pulse duration t_p . Since I_c determines the oscillation frequency, the pulse can end up in different oscillation states, causing positive or negative drift. This can strongly change $\langle v_{DW} \rangle$ and causes DW motion against the current direction for small I_c .

VI. CONCLUSIONS

In this paper, we have shown that Rashba spin-orbit interactions can qualitatively affect the current-driven DW motion in ferromagnetic nanowires. Their main influence is encoded in a nonequilibrium Rashba field H_R , which is responsible for magnetization precession and thereby for qualitative changes in the DW dynamics. Remarkably, we find that the conspiracy of spin relaxation and spin-orbit coupling is able to generate a dominant contribution to H_R even for weak Rashba couplings. As a consequence, above a critical current-induced Rashba field $H_R > H^{WB}$, the DW dynamics is predicted to exhibit oscillatory features (similar to the field-driven case above the Walker breakdown) and a nontrivial dependence of the DW velocity on the current density. In fact, the DW motion can turn from a purely translational into an oscillatory dynamics due to precession of the DW magnetization around the local nonequilibrium Rashba field. When using pulsed currents with variable pulse duration, even the direction of the DW motion can be controlled. All predicted effects should be observable with present-day experimental techniques.

ACKNOWLEDGEMENTS

We thank Guido Meier for helpful discussions. M. T. thanks M. Preuninger for support. We acknowledge support from the SFB 668 (Project B16) and from the SFB TR 12 of the DFG.

Appendix: Detailed calculations and magnetization profile

Here we provide a detailed derivation of the spin torque quoted in the main text and give the expressions valid for arbitrary Rashba coupling α_R . In addition, we briefly discuss the space-time profile of the magnetization.

1. Derivation of the spin torque

Since we treat a nanowire in the one-dimensional (1D) limit, we employ a Luttinger liquid (LL) description for the itinerant electrons. While there are several representations for the LL Hamiltonian, we choose the Sugawara formulation which is most convenient here. As discussed in textbooks²⁶, after linearization of the spectrum, the spin sector of the kinetic energy is encoded in the universal spin Hamiltonian $H_0 = \sum_p \frac{v}{2} \int dx : \mathbf{J}_p \cdot \mathbf{J}_p :$, where $:\dots:$ stands for normal ordering, v is the spin velocity (which essentially equals the Fermi velocity), and the chiral spin density operators are

$$\mathbf{J}_p(x) = \frac{1}{2} : c_{p\sigma}^\dagger(x) \boldsymbol{\sigma}_{\sigma\sigma'} c_{p\sigma'}(x) :$$

for left- and right-movers ($p = R, L = +, -$), respectively^{26,34}. The 1D fermion operators $c_{p,\sigma}(x)$ describe a p -mover with spin projection σ , and $\boldsymbol{\sigma}$ is the vector of spin Pauli matrices. The spin density operator is then given by $\mathbf{s} = \mathbf{J}_R + \mathbf{J}_L$. Similarly, chiral density operators are introduced as $j_p = \sum_\sigma c_{p,\sigma}^\dagger c_{p,\sigma}$, with expectation value $\langle j_p \rangle = \rho_p$. The particle density is $\rho_c = \sum_p \rho_p$, and the current density is given by $I_c = ev \sum_p p \rho_p$. The above description also applies when Coulomb interactions are important²⁶.

Within the low-energy LL approach, particles are constrained to have 1D momenta close to $k_x \approx pk_F$ with Fermi wavenumber k_F . This fact allows us to simplify the standard two-dimensional Rashba spin-orbit single-particle Hamiltonian, $\tilde{\alpha}_R(\sigma_y k_x - \sigma_x k_y)$ with Rashba coupling $\tilde{\alpha}_R$, by effectively putting $k_x \rightarrow pk_F$ and $k_y \rightarrow 0$. With the dimensionless Rashba coupling $\alpha_R = 2\tilde{\alpha}_R k_F / \Delta_{sd}$ and using the definition of \mathbf{J}_p , we arrive at the second-quantized form

$$H_{SOI} = \Delta_{sd} \alpha_R \sum_p \int dx \mathbf{J}_p \cdot \mathbf{e}_y. \quad (\text{A.1})$$

Adding the sd Hamiltonian, $H_{sd} = \Delta_{sd} \int dx \mathbf{s} \cdot \mathbf{n}$, describing the exchange interaction between the magnetization \mathbf{n} and the spin density $\mathbf{s} = \mathbf{J}_R + \mathbf{J}_L$ of the itinerant electrons, we arrive at the Hamiltonian

$$H_{el} = H_0 + \Delta_{sd} \sum_{p=\pm} \int dx \mathbf{J}_p \cdot (\mathbf{n} + p\alpha_R \mathbf{e}_y). \quad (\text{A.2})$$

The spin torque, $\mathbf{T} = -\Delta_{sd} \mathbf{n} \times \langle \mathbf{s} \rangle$, entering the LLG equation can then be calculated by solving the Heisen-

berg equations of motion (EOM) for \mathbf{J}_p . With the standard summation convention, these operators obey the Kac-Moody algebra²⁶

$$[J_p^a(x), J_{p'}^b(x')]_- = ip\delta^{ab}\delta^{pp'}\partial_x\delta(x-x') + i\delta^{pp'}\epsilon^{abc}J_p^c\delta(x-x'),$$

with the Kronecker symbol δ^{ab} and the Levi-Civita symbol ϵ^{abc} . The Heisenberg EOM then reads

$$\partial_t\mathbf{J}_p + pv\partial_x\mathbf{J}_p = -\Delta_{sd}\mathbf{J}_p \times (\mathbf{n} + p\alpha_R\mathbf{e}_y),$$

where a term $\propto \partial_x\mathbf{n}$, irrelevant to the following discussion, has been omitted. Itinerant electron spins are also subject to relaxation processes not captured by the above Hamiltonian, e.g., due to quasi-elastic or magnetic disorder effects and/or additional spin-orbit coupling mechanisms. In this work, we model relaxation on phenomenological grounds by adding relaxation terms to the EOM:

$$\partial_t\mathbf{J}_p + pv\partial_x\mathbf{J}_p = -\Delta_{sd}\mathbf{J}_p \times (\mathbf{n} + p\alpha_R\mathbf{e}_y) - \sum_{\nu=i,ii} \beta^{(\nu)}\Delta_{sd}(\mathbf{J}_p - \mathbf{J}_p^{(\nu)}). \quad (\text{A.3})$$

The index ν stands for different relaxation channels. Each channel is characterized by the rate $\beta^{(\nu)}\Delta_{sd}$ and a corresponding quasi-stationary state $\mathbf{J}_p^{(\nu)}(x,t)$ that the system tries to reach. We here include two relevant channels: One ($\nu = i$) is provided by the externally imposed spin-polarized current $I_s = \hbar PI_c/(2e)$, where a p -mover has density ρ_p and the spin polarization factor is P , with $|P| \leq 1$. This implies the stationary distribution $\mathbf{J}_p^{(i)} = (P\rho_p/2)\mathbf{n}$. The second mechanism ($\nu = ii$) describes intrinsic relaxation to the stationary solution of Eq. (A.3), $\mathbf{J}_p^{(ii)} = (P\rho_p/2)[\mathbf{n} + p\alpha_R\mathbf{e}_y]$.

In order to solve Eq. (A.3) for the physically relevant case of slow space-time variation of the magnetization,

we now perform an iterative gradient expansion. In this approach⁵, \mathbf{J}_p is expanded in orders of derivatives of the magnetization unit vector $\mathbf{n}(x,t)$, $\mathbf{J}_p = \sum_{k=0}^{\infty} \mathbf{J}_p^{(k)}$, where $\mathbf{J}_p^{(k)}$ depends on space-time derivatives of \mathbf{n} of k th order only. With this, the EOM (A.3) can be rearranged according to orders of k , allowing for an iterative solution. In this scheme, we first solve the $k = 0$ equations, then use this solution to obtain the $k = 1$ term, and so on. In particular, for $k = 0$, we have to solve

$$0 = -\Delta_{sd}\mathbf{J}_p^{(0)} \times (\mathbf{n} + p\alpha_R\mathbf{e}_y) - \sum_{\nu=i,ii} \beta^{(\nu)}\Delta_{sd}(\mathbf{J}_p^{(0)} - \mathbf{J}_p^{(\nu)}). \quad (\text{A.4})$$

The k th-order contribution to the spin torque, $\mathbf{T}^{(k)}$, then follows from

$$\mathbf{T} = \sum_{k=0}^{\infty} \mathbf{T}^{(k)}, \quad \mathbf{T}^{(k)} = -\Delta_{sd}\mathbf{n} \times \sum_p \mathbf{J}_p^{(k)}.$$

For sufficiently smooth space-time variation of the magnetization, the lowest few orders capture the relevant physics. Due to the complexity of the higher-order terms, we here restrict the calculations to zeroth and first order terms.

2. Results for the spin torque

As outlined above, we have $\mathbf{T}(x,t) = \mathbf{T}^{(0)} + \mathbf{T}^{(1)}$, where the first term involves no space-time derivatives $\partial_{x,t}\mathbf{n}$ and the second contains exactly one first-order derivative. Some algebra yields $\mathbf{T}^{(0)} = \mathbf{T}_1 + \mathbf{T}_2$ with

$$\begin{aligned} \mathbf{T}_1 &= \frac{\Delta_{sd}\alpha_R}{v\mathcal{N}} \left\{ -I_s \left[1 + \alpha_R^2(1 - 2n_y^2) + \frac{\beta^{(ii)}}{\beta^{(i)} + \beta^{(ii)}}\alpha_R^2(1 - 2n_y^2 + \alpha_R^2) \right] \right. \\ &\quad \left. + \rho_s v \frac{\beta^{(ii)}}{\beta^{(i)} + \beta^{(ii)}}\alpha_R n_y (\alpha_R^2 - 1) \right\} \mathbf{n} \times \mathbf{e}_y, \\ \mathbf{T}_2 &= \beta^{(i)} \frac{\Delta_{sd}\alpha_R}{v\mathcal{N}} [I_s(1 + \alpha_R^2) + 2\rho_s v\alpha_R n_y] \mathbf{n} \times (\mathbf{n} \times \mathbf{e}_y), \\ \mathcal{N} &= (1 + \alpha_R^2)^2 - 4\alpha_R^2 n_y^2, \end{aligned}$$

where $\rho_s = P\rho_c/(2e)$. We stress that these results are valid for arbitrary α_R . We also provide explicit expressions for the next order:

$$\mathbf{T}^{(1)} = \mathcal{N}^{-2} \sum_{\nu=x,t} (A_\nu \partial_\nu \mathbf{n} + B_\nu \mathbf{n} \times \partial_\nu \mathbf{n}) - H_R^{(1)} \mathbf{n} \times \mathbf{e}_y$$

with

$$\begin{aligned}
(\beta^{(i)} + \beta^{(ii)})A_t &= -\frac{I_s}{v}(\alpha_R^2 - 1)\alpha_R n_y \left\{ \beta^{(ii)}\mathcal{N} - 2\beta^{(i)} [1 - \alpha_R^4 + 2\alpha_R^2(\alpha_R^2 - 1)n_y^2] \right\} \\
&\quad + \rho_s \left\{ -\beta^{(ii)}\mathcal{N} [1 + \alpha_R^2(1 - 2n_y^2)] - \beta^{(i)} [\mathcal{N} + \alpha_R^2 n_y (8\alpha_R^2(n_y^2 - 1) - \mathcal{N})] \right\}, \\
(\beta^{(i)} + \beta^{(ii)})A_x &= I_s \left\{ -\beta^{(ii)}\mathcal{N} [1 + \alpha_R^2(1 - 2n_y^2)] - \beta^{(i)} [\mathcal{N} + \alpha_R^2 n_y (8\alpha_R^2(n_y^2 - 1) - \mathcal{N})] \right\} \\
&\quad - \rho_s v (\alpha_R^2 - 1) \alpha_R n_y \left\{ \beta^{(ii)}\mathcal{N} + 2\beta^{(i)} [1 + \alpha_R^2(1 - 2n_y^2)] \right\}, \\
B_t &= \frac{I_s \alpha_R n_y}{v} \left[4\beta^{(i)}(\alpha_R^4 - 1) + 2\beta^{(ii)}\mathcal{N} \right] + \rho_s \mathcal{N} \left[\beta^{(ii)}(1 + \alpha_R^2) + \beta^{(i)}(\alpha_R^2 - 1) \right], \\
B_x &= I_s \beta^{(i)}(1 - \alpha_R^2)(\mathcal{N} + 8\alpha_R^2 n_y^2) + 4\rho_s v \beta^{(i)} \alpha_R n_y (\alpha_R^4 - 1),
\end{aligned}$$

and

$$\begin{aligned}
H_R^{(1)} &= \mathcal{N}^{-2} \sum_{\nu=x,t} (h_\nu \partial_\nu n_y + h'_\nu \partial_\nu \mathbf{n} \cdot (\mathbf{n} \times \mathbf{e}_y)), \\
(\beta^{(i)} + \beta^{(ii)})^2 h_t &= -\frac{I_s \alpha_R^3 n_y}{v} \left\{ 2\beta^{(ii)}\mathcal{N} + \beta^{(i)} [-1 + 3\alpha_R^4 + 2\alpha_R^2(1 - 2n_y^2)] \right\} \\
&\quad - \rho_s \alpha_R^2 \left\{ \beta^{(i)} \alpha_R^2 [(1 + \alpha_R^2)^2 - 4n_y^2] + \beta^{(ii)}(1 + \alpha_R^2)\mathcal{N} \right\}, \\
(\beta^{(i)} + \beta^{(ii)})^2 h_x &= -I_s \alpha_R^2 \left[\beta^{(ii)}(1 + \alpha_R^2)\mathcal{N} + \beta^{(i)} \alpha_R n_y \mathcal{N} \right] \\
&\quad + \rho_s v \alpha_R^3 n_y \left\{ 2\beta^{(ii)}\mathcal{N} + \beta^{(i)} [-1 + 3\alpha_R^4 + 2\alpha_R^2(1 - 2n_y^2)] \right\}, \\
(\beta^{(i)} + \beta^{(ii)})h'_t &= -4\beta^{(i)} \frac{I_s}{v} n_y \alpha_R^3 (1 + \alpha_R^2) + \beta^{(i)} \rho_s \alpha_R^2 (\mathcal{N} + 8\alpha_R^2 n_y^2), \\
(\beta^{(i)} + \beta^{(ii)})h'_x &= \beta^{(i)} I_s [(\alpha_R + \alpha_R^3)^2 + 4\alpha_R^2 n_y^2] - 4\beta^{(i)} \rho_s \alpha_R^3 n_y (1 + \alpha_R^2).
\end{aligned}$$

3. Time-dependent magnetization profile

When the Rashba field exceeds a distinct value, the magnetization starts to precess around the axis defined by the field, in this case the y -axis. Let us illustrate such a scenario, see Fig. 6. As long as a spin-polarized current I_s flows, a nonequilibrium Rashba field is created, which

then causes precession of the magnetization \mathbf{n} around this field. The resulting precession period equals two periods of the velocity variation, cf. Fig. 3. When the current is switched off (not shown in the figure), the DW relaxes slowly back to its stationary state, i.e., the state for $t = 0$ in the figure.

¹ L. Berger, J. Appl. Phys. **49**, 2156 (1978).

² C. H. Marrows and G. Meier, Special Issue on *Domain wall dynamics in nanostructures*, J. Phys.: Condens. Matter **24**, 020301 (2012).

³ S. Zhang and Z. Li, Phys. Rev. Lett. **93**, 127204 (2004).

⁴ Y. Tserkovnyak, H.J. Skadsem, A. Brataas, and G.E.W. Bauer, Phys. Rev. B **74**, 144405 (2006).

⁵ M. Thorwart and R. Egger, Phys. Rev. B **76**, 214418 (2007).

⁶ G. Tatara, H. Kohno, and J. Shibata, Phys. Rep. **468**, 213 (2008).

⁷ I. Garate, K. Gilmore, M.D. Stiles, and A.H. MacDonald, Phys. Rev. B **79**, 104416 (2009).

⁸ M. Hayashi, L. Thomas, C. Rettner, R. Moriya, Y.B. Bazaliy, and S.S.P. Parkin, Phys. Rev. Lett. **98**, 037204 (2007).

⁹ G. Meier, M. Bolte, R. Eiselt, B. Krüger, D.H. Kim, and P. Fischer, Phys. Rev. Lett. **98**, 187202 (2007).

¹⁰ K. Obata and G. Tatara, Phys. Rev. B **77**, 214429 (2008).

¹¹ A. Manchon and S. Zhang, Phys. Rev. B **78**, 212405 (2008); Phys. Rev. B **79**, 094422 (2009).

¹² I.M. Miron, T. Moore, H. Szabolics, L.D. Buda-Prejbeanu, S. Auffret, B. Rodmacq, S. Pizzini, J. Vogel, M. Bonfim, A. Schuhl, and G. Gaudin, Nature Mat. **10**, 419 (2011).

¹³ We focus on the Rashba case, but the Dresselhaus SOI gives essentially the same physics, see: A. Matos-Abiad and R.L. Rodriguez-Suarez, Phys. Rev. B **80**, 094424 (2009).

¹⁴ I.M. Miron, G. Gaudin, S. Auffret, B. Rodmacq, A. Schuhl, S. Pizzini, J. Vogel, and P. Gambardella, Nature Mat. **9**, 230 (2010).

¹⁵ I.M. Miron, K. Garello, G. Gaudin, P.J. Zermatten, M.V. Costache, S. Auffret, S. Bandiera, B. Rodmacq, A. Schuhl, and P. Gambardella, Nature **476**, 189 (2011).

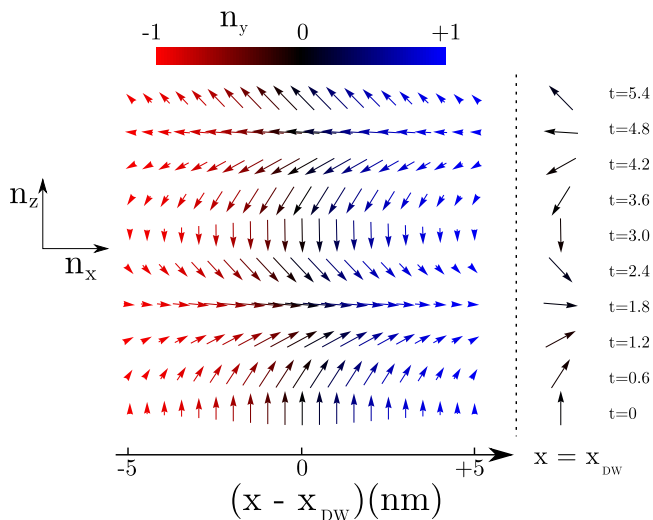


FIG. 6. (Color online) The magnetization profile in the vicinity of the DW center $x \approx x_{DW}$ at different times t (in nanoseconds, from the bottom to the top). Arrows indicate $n_{x,z}(x - x_{DW}, t)$, while n_y is color-coded. For clarity, we show the magnetization profile right at the DW center $x = x_{DW}$ in a separate column on the right of the profile. Due to the finite Rashba field, the magnetization precesses around the y -axis, i.e., the direction of the Rashba field. Parameters are as in Fig. 3 for constant current.

- ¹⁶ J. Ryu, S.B. Choe, and H.W. Lee, Phys. Rev. B **84**, 075469 (2011).
¹⁷ M. Hayashi, Y. Nakatani, S. Fukami, M. Yamanouchi, S. Mitani, and H. Ohno, J. Phys.: Cond. Matter **24**, 024221 (2012).

- ¹⁸ J. Ryu, S.M. Seo, K.J. Lee, and H.W. Lee, J. Magn. Magn. Mat. **324**, 1449 (2012).
¹⁹ E. Martinez, J. Appl. Phys. **111**, 07D302 (2012).
²⁰ K. Tsutsui and S. Murakami, Phys. Rev. B **86**, 115201 (2012).
²¹ K.W. Kim, S.M. Seo, J. Ryu, K.J. Lee, and H.W. Lee, Phys. Rev. B **85**, 180404(R) (2012).
²² X. Wang and A. Manchon, Phys. Rev. Lett. **108**, 117201 (2012).
²³ D.A. Pesin and A.H. MacDonald, Phys. Rev. B **86**, 014416 (2012).
²⁴ E. van der Bijl and R.A. Duine, Phys. Rev. B **86**, 094406 (2012).
²⁵ X. Wang, C.O. Pauyac, and A. Manchon, arXiv:1206.6726.
²⁶ A.O. Gogolin, A.A. Nersisyan, and A.M. Tsvelik, *Bosonization and Strongly Correlated Systems* (Cambridge University Press, 1998).
²⁷ R. Winkler, *Spin-orbit coupling effects in two-dimensional electron and hole systems* (Springer, Berlin, 2003).
²⁸ S. Gangadharaiah, J. Sun, and O. A. Starykh, Phys. Rev. B **78**, 054436 (2008).
²⁹ D.H. Hernando, Y.V. Nazarov, A. Brataas, and G.E.W. Bauer, Phys. Rev. B **62**, 5700 (2000).
³⁰ L. Balents and R. Egger, Phys. Rev. B **64**, 035310 (2001).
³¹ The Rashba term $H_R^{(1)}$ obviously diverges for $\beta^{(i)} + \beta^{(ii)} \rightarrow 0$ in this simplified relaxation time approximation. This appears to be unphysical and can be resolved by including higher orders than linear in $\beta^{(i,ii)}$ for the relaxation dynamics⁵. We exclude this limiting case from our discussions.
³² L. Thomas and S. Parkin, in *Handbook of Magnetism and Advanced Magnetic Materials*, ed. by H. Kronmüller and S. Parkin (John Wiley & Sons, 2007).
³³ J. Vogel, M. Bonfim, N. Rougemaille, O. Boulle, I.M. Miron, S. Auffret, B. Rodmacq, G. Gaudin, J.C. Cezar, F. Sirotti, and S. Pizzini, Phys. Rev. Lett. **108**, 247202 (2012).
³⁴ P. Fröjdh and H. Johannesson, Phys. Rev. B **53**, 3211 (1996).